

Article

Enhanced Performance of a Supercapacitor by Addition of Turbostratic Fractal Graphene to an Activated Carbon Electrode

Maithri Dissanayake¹, Charlie Karunaratne¹, A. V. R. S. Koswaththa², S. G. S. M. Nawarathna², M. I. U. Weerasinghe³, G. R. A. Kumara³, and Ranjith Divigalpitiya^{4,*}

¹ VolfPack Energy Ltd., Colombo 03, Sri Lanka

² Faculty of Science, University of Peradeniya, Peradeniya, Kandy 20400, Sri Lanka

³ National Institute of Fundamental Studies, Hantana, Kandy 20000, Sri Lanka

⁴ HydroGraph Clean Power Inc., 1199 W. Hastings St. #110, Vancouver, BC V6E 3T5, Canada

* Correspondence: ranjith.divigalpitiya@hydrograph.com

Received: 19 November 2024; Revised: 24 December 2024; Accepted: 08 February 2025; Published: 24 March 2025

Abstract: This research explores the enhancement of supercapacitor performance through the incorporation of a new form of turbostratic graphene (Fractal Graphene, FGA-1) into activated carbon (AC) electrodes. By combining FGA-1 with AC, the electrodes exhibit improved electrical conductivity and enhanced electrolyte diffusion, leading to superior charge storage capability. Material characterization confirms that the FGA-1–AC composite forms a synergistic structure, facilitating better interaction with the electrolyte. The composite electrodes demonstrate significant improvements in specific capacitance compared to AC-only counterparts. Enhanced wettability and optimized diffusion rates were identified as key factors contributing to these improvements. The findings highlight the potential of FGA-1 as an additive for improving the efficiency of carbon-based supercapacitors, providing a foundation for high-performance energy storage solutions suitable for a broad range of applications.

Keywords: activated carbon; energy storage devices; Fractal Graphene; turbostratic; supercapacitors; wettability

1. Introduction

In recent decades, the depletion of fossil fuels and escalating environmental concerns have spurred significant interest in renewable energy. Researchers have been working on cost-effective, energy-efficient, and eco-friendly energy sources and storage devices to meet this growing demand [1]. This shift has also resonated in the business sector, where sustainability and environmental protection increasingly drive policy and investment decisions [2].

Several factors underscore the transformation of modern power systems, including the need for self-sufficient microgrids, reductions in CO₂ emissions, and responsiveness to rapidly changing energy requirements. These trends highlight the necessity of fully sustainable energy storage solutions [3]. Solar, wind, hydro, and geothermal power all show great promise, but their intermittent generation profiles require robust storage to balance the grid. As the share of renewables approaches 80%, the demand for large-scale, flexible energy storage will inevitably increase [4,5].

Electrochemical energy storage systems—such as lithium-ion (Li-ion) batteries, sodium-ion (Na-ion) batteries, and supercapacitors—are among the leading technologies under investigation. Li-ion batteries have found widespread use, from portable electronics to electric vehicles [6]. In parallel, supercapacitors (SCs), sometimes called ultracapacitors, have attracted attention because of their long cycle life, high power density, rapid charge–discharge capabilities, high Coulombic efficiency, and simplified estimation of the state of charge (SoC) [7–9].

Supercapacitors can be classified into three categories—electric double-layer capacitors (EDLCs), pseudocapacitors, and hybrid capacitors—based on their respective energy storage mechanisms [10–12]. EDLCs, which store charge electrostatically, stand out for their long cycle life, low cost per cycle, and low internal resistance [13]. Pseudocapacitors, in contrast, rely on redox-active materials like metal oxides or conducting polymers [14–16]. Despite extensive research into advanced carbon materials such as carbon nanotubes or



graphene, the large-scale performance of EDLC-based devices has often fallen short, owing to lower-than-expected specific capacitance and scalability challenges [17,18].

In recent years, efforts to enhance supercapacitors have focused on graphene and its derivatives. For example, graphene-activated carbon electrodes have been shown to offer higher energy and power densities compared to activated carbon alone [1,19,20]. One promising strategy is improving the wettability of the electrode surface, which facilitates ion mobility and can boost specific capacitance by up to 17.8% [21–23]. Heteroatom doping is another pathway, introducing polar sites that enhance both wettability and conductivity [24,25].

A novel form of graphene, known as Fractal Graphene, is manufactured by HydroGraph using a “Chamber Detonation” process—an adaptation of detonation synthesis—to produce pristine graphene powder (carbon content > 99%) on a commercial scale [26,27]. Originally developed by Prof. Christopher Sorensen at Kansas State University, this method involves detonating gaseous mixtures of oxygen and acetylene at varying oxygen-to-carbon (O/C) molar ratios (0.25–0.75) using an electrical spark. The process generates transient pressures above 190 psi and temperatures above 2430 K, creating nano-sized (20–50 nm) particles of few-layer graphene in a reproducible manner. The resulting graphene exhibits a turbostratic structure—where the individual layers are stacked randomly—and is free of metallic impurities due to the absence of catalysts [26,27].

Detailed characterization by Raman spectroscopy, X-ray diffraction (XRD), Brunauer–Emmett–Teller (BET) surface area analysis, scanning electron microscopy (SEM), and transmission electron microscopy (TEM) in earlier references confirms that this detonation approach reliably yields high-purity, turbostratic graphene [26,27]. Because Fractal Graphene Aggregates (FGA-1) are electrically conductive, their branched network of primary graphene particles can enhance conductivity in composites. This characteristic is particularly advantageous in supercapacitor electrodes, where high purity is crucial to minimize side reactions during charging and discharging. Thus, Fractal Graphene shows strong potential as a conductive additive in activated carbon-based supercapacitor electrodes.

In this study, we demonstrate a straightforward route to improve the performance of activated carbon-based supercapacitors by incorporating this new type of graphene. We investigate the influence of Fractal Graphene on electrolyte ion diffusion and assess its subsequent impact on the overall performance of supercapacitor devices.

2. Experimental

2.1. Materials

Fractal Graphene (FGA-1) was obtained from HydroGraph Clean Power Inc., Toronto, ON, Canada) Other materials included tetraethylammonium tetrafluoroborate (TEABF₄; Acros Organics, Maharashtra, India), activated carbon (AC; Haycarb, Colombo, Sri Lanka), polyvinylpyrrolidone (PVP; Sigma-Aldrich, MI, USA), isopropyl alcohol (IPA; Chem-Lab, Zedelgem, Belgium), acetonitrile (ACN; Research Lab Fine Chem Industries, Maharashtra, India), and a cellulose separator (NKK-4530, Nippon Kodoshi Corporation, Kochi, Japan).

2.2. Instrumentation

X-ray diffraction (XRD) measurements were performed using a Rigaku Ultima IV diffractometer equipped with a Cu anode and dual detectors. The specific surface area was determined by the BET method on a Quantachrome® ASiQwin™ instrument. The morphology and structure of the samples were examined with a Zeiss EVO 15 scanning electron microscope (SEM). Optical properties were investigated via UV-Vis spectroscopy using a Shimadzu 2450 spectrophotometer. The chemical structure, crystallinity, and molecular structure were analyzed by Raman spectroscopy on a Renishaw InVia system with a 514 nm laser. Cyclic voltammetry (CV) was carried out using a two-electrode setup on a VK-PA-300 electrochemical workstation. GCD (galvanostatic charge–discharge) experiments were carried out using a Metrohm Autolab PGSTAT 128 N, and electrochemical impedance spectroscopy (EIS) was conducted with the same system using FRA (Frequency Response Analysis) software.

2.3. Device Fabrication and Electrochemical Testing

FGA-1 and AC powders were dried at 150 °C for 30 min to remove moisture. Next, 0.20 g FGA-1 (4% by mass) and 5.00 g AC were mixed in a disk mill for 5 min. Then, 0.20 g PVA was added, followed by stepwise addition of 25 mL IPA. The resulting slurry was stirred at 900 rpm for 20 min. Electrodes were prepared by spray-pyrolyzing the slurry onto stainless steel substrates on a 150 °C hot plate, then sintered at 300 °C for 20 min. The final electrodes were composed of 96 wt% active material (AC + FGA-1) and 4 wt% binder (PVP), cut to dimensions of 5.00 cm × 4.00 cm.

For supercapacitor assembly, two electrodes were separated by an NKK separator. A 1 M TEABF₄ solution in ACN was used as the electrolyte. The cell was gently pressed to ensure proper electrical connection.

Capacitance values of the supercapacitors at various scan rates were determined by cyclic voltammetry (CV) in a two-electrode configuration using a VK-PA-300 electrochemical workstation. The specific capacitance (in F g⁻¹) was calculated from CV data by integrating the charge–discharge curves (recorded on a Metrohm Autolab PGSTAT 128 N) over a potential range of 0–2.0 V. Electrochemical impedance spectroscopy (EIS) measurements were conducted on the same system with the FRA software, and the resulting Nyquist plots were fitted using the built-in NOVA software (Ver. 2.1.7).

3. Results and Discussion

3.1. Optical, Structural, and Morphological Studies

3.1.1. Optical Characterization

Figure 1 shows the UV-Vis absorption spectra of AC, FGA-1, and their composite. AC exhibits a peak at 199.4 nm with an absorbance of 0.205, FGA-1 peaks at 202.2 nm with an absorbance of 0.397, and AC:FGA-1 composite peaks at 190.4 nm, showing an absorbance of 0.593. Notably, the composite's absorbance (0.593) nearly matches the sum of the individual absorbances (0.602), suggesting that the composite behaves as an independent material [28].

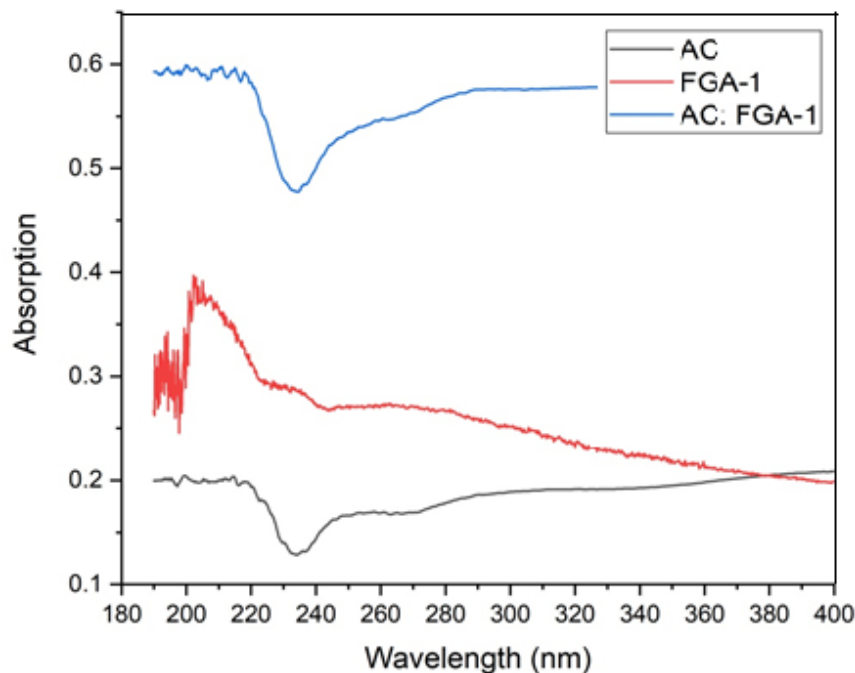


Figure 1. UV-Vis spectra of AC, FGA-1, and the AC:FGA-1 composite.

3.1.2. Morphological Characterization

SEM images of AC, FGA-1, and AC:FGA-1 (Figure 2) reveal that AC has irregular, jagged particles, while FGA-1 appears as agglomerates. In the composite (Figure 2c–f), FGA-1 nanoparticles seem to bridge AC particles, covering pores and edges. This bridging likely improves both the wettability and the electrical conductivity of the electrode.

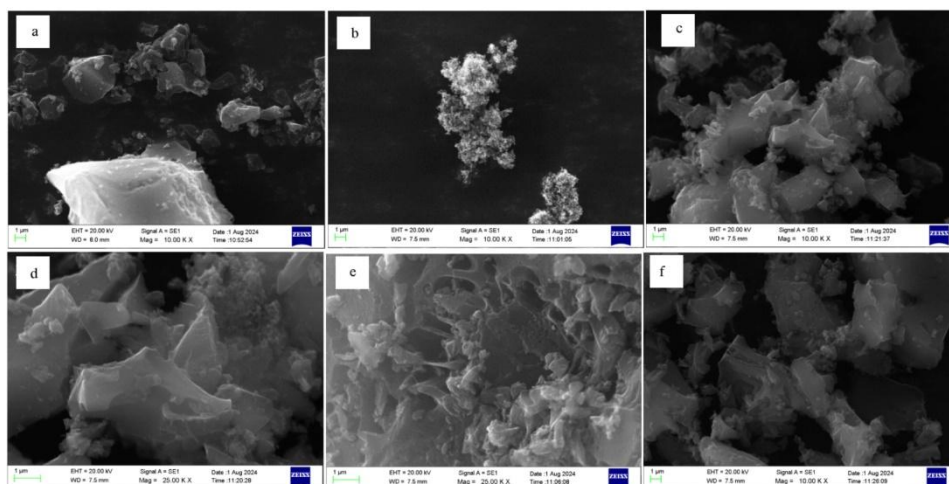


Figure 2. SEM images of (a) AC, (b) FGA-1, and (c–f) AC:FGA-1 composite.

3.1.3. Structural Characterization

XRD patterns for AC, FGA-1, and the AC:FGA-1 composite appear in Figure 3. Each pattern shows two broad peaks near 19° and 43°, corresponding to the (002) and (100) planes of graphite (JCPDS 00-056-0159). Table 1 summarizes the crystallite parameters. The shift observed in the (002) peak of the composite appears to result from the overlapping of the broad, amorphous peak from AC with the sharper FGA-1 peak. Because the mixture process is relatively benign, major structural changes to FGA-1 are unlikely [29].

Table 1. XRD microcrystalline parameters of the materials.

Materials	2θ ₀₀₂ (°)	2θ ₁₀₀ (°)	d ₀₀₂ (nm)	d ₁₀₀ (nm)
AC	19.16	43.82	0.46	0.21
FGA-1	25.35	43.11	0.35	0.21
AC:FGA-1	22.6	43.56	0.39	0.21

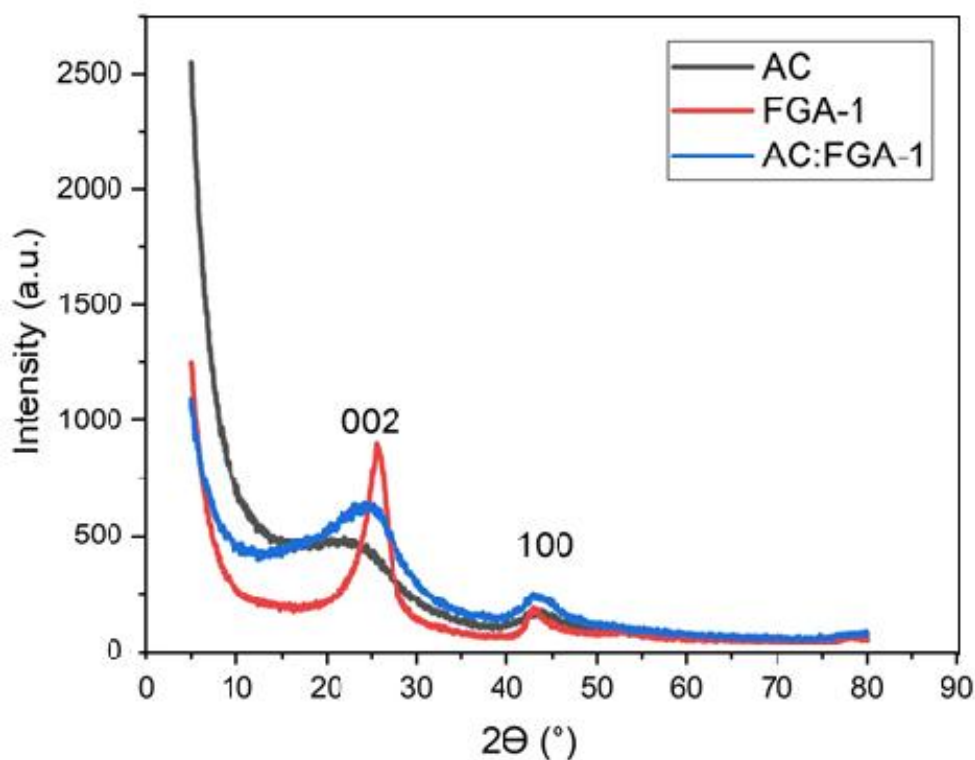


Figure 3. XRD patterns of AC, FGA-1, and the AC:FGA-1 composite.

Figure 4 and Table 2 present the Raman spectra and D/G band fitting parameters. The D band ($\sim 1330\text{--}1340\text{ cm}^{-1}$) indicates disorder, while the G band ($\sim 1570\text{--}1600\text{ cm}^{-1}$) is characteristic of graphitic sp^2 -hybridized carbon [30]. The ratio of intensities (I_D/I_G) provides a measure of structural disorder. AC shows $I_D/I_G = 0.86$, whereas FGA-1's 1.19 indicates a higher defect concentration, likely due to its turbostratic, nano-sized nature [31–33]. The composite's $I_D/I_G = 0.93$ lies between those of its constituents.

Table 2. Raman band positions and intensities for AC, FGA-1, and the composite.

Material	D (cm^{-1})	G (cm^{-1})	I_G	I_D	I_D/I_G
AC	1340	1599	901.47	776.73	0.86
FGA-1	1340	1570	944.23	1130.64	1.19
AC:FGA-1	1330	1596	2264.59	2102.96	0.93

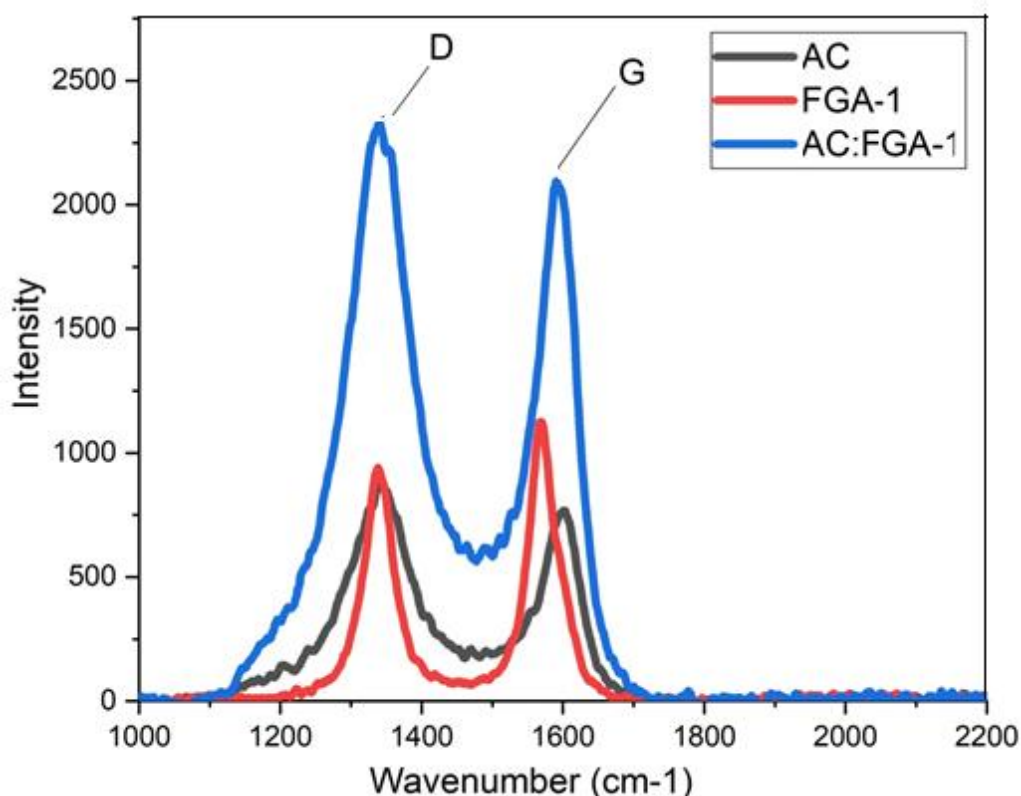


Figure 4. Raman spectra of AC, FGA-1, and AC:FGA-1, showing D and G bands.

3.2. Study of Effective Diffusion Rates of Electrolytes in Activated Carbon with FGA-1

To investigate how FGA-1 affects electrolyte diffusion, we measured the distance traveled by the electrolyte in a fixed time (120 s) when placed in pure AC and in an AC:FGA-1 mixture as follows.

Two test tubes were marked in millimeters for the measurement (Figure 5). One test tube was filled with activated carbon (AC), while the other was filled with a composite of FGA-1 and AC, after ensuring a thorough blending beforehand. A pipette was used to dispense exactly 20 drops of electrolyte solution into each test tube. Each drop was confirmed to have a volume of 0.0285 mL. A stopwatch was started simultaneously for both test tubes, and the test proceeded for two minutes (120 s). During this time, the distance traveled by the electrolyte was monitored and recorded. This procedure was repeated with different number of drops of electrolyte.

Table 3 summarizes the distances observed in each mixture over the 120 s for different volumes.

The data is plotted (the distance travelled as a function of number of droplets) to check if there is an effect of the volume of added electrolyte (Figure 6).

We note that the FGA-1:AC mixture displayed a higher diffusion rate compared to AC alone. As illustrated in Figure 6 and Table 3, the electrolyte penetrates the composite roughly twice as far compared to AC alone, indicating faster diffusion.



Figure 5. Experimental setup for observing diffusion rates of electrolyte in electrode materials.

This observation is consistent with the Washburn equation [34], which shows that the wettability (characterized by contact angle and pore structure) plays a critical role in liquid infiltration. We propose that the enhanced wettability in the AC:FGA-1 composite leads to improved capillary penetration, explaining the nearly doubled diffusion distance.

Table 3. Distance traveled by the electrolyte in 120 s in AC vs. AC:FGA-1 composite.

Number of Drops (0.0285 mL/drop)	Distance Travelled (AC only) L ₁ (cm)	Distance Travelled (Hydrograph+ AC) L ₂ (cm)	L ₁ /L ₂
20	0.7	1.5	2.1
40	1.1	2.1	1.9
60	1.6	2.8	1.8
80	2	3.8	1.9
100	2.5	5	2.0
Average ± std. deviation			1.9 ± 0.1

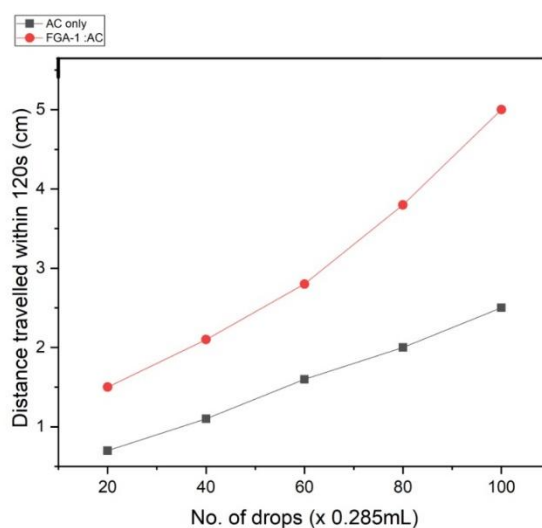


Figure 6. Distance traveled by the electrolyte in AC vs. AC:FGA-1 over 120 s.

We define an effective diffusion constant, $D = L^2/t$, to quantify this effect (Equation (1)), where L represents the average distance traveled by the electrolyte in our experiment, and t is the fixed time duration of 2 min. The effective diffusion constants of activated carbon with and without the addition of Fractal Graphene was then compared. This comparison was achieved using the ratio D_1/D_2 , where D_1 represents the effective diffusion constant with Fractal Graphene (enhanced) and D_2 represents the diffusion constant without Fractal Graphene (base case).

$$\frac{D_1}{D_2} = \left(\frac{L_1}{L_2}\right)^2 \quad (1)$$

Our data indicate that the ratio of the diffusion constants, D_1/D_2 , (with FGA-1 and without FGA-1) is ~ 4 , implying a fourfold increase in effective diffusion when FGA-1 is added. This improvement in electrolyte penetration suggests that more of the active surface area is accessible, potentially leading to higher capacitance in supercapacitor applications [35,36].

These findings offer significant potential for developing improved supercapacitor materials. The basic mechanism of supercapacitors—forming an electrical double layer (EDL)—depends on adequately wetting the conductive surface of the electrode's active material, which ensures efficient electrolyte penetration and charge storage. Poor wettability limits the effective use of the available surface area, resulting in lower specific capacitance. Consequently, enhancing wettability increases the specific capacitance and thereby raises the energy density, even when the material and structure remain the same [35]. For large-scale manufacturing, the slow electrolyte filling process during supercapacitor fabrication can also pose challenges [36]. In our experiments, we have demonstrated evidence of faster electrolyte penetration in the FGA-1 mixed AC electrode.

For comparison, the literature reported specific capacitance of an activated carbon-based supercapacitor falls between 50 and 200 F g⁻¹, and the value strongly depends on the kind of activation and structural properties of the carbon used [37].

3.3. Electrical Characterization

The electrochemical characterization of the supercapacitors was conducted using a two-electrode configuration as detailed in the experimental section. The specific capacitance of the system was calculated using Equation (2) [38].

$$C = \frac{1 \int I dv}{2m \Delta V \frac{dv}{dt}} \quad (2)$$

where m is the mass of the activated carbon layer on the electrode surface, I is current, ΔV is the potential range used and dv/dt is the potential scan rate used for the CV experiment.

Figure 7 shows how total capacitance varies with different loadings of FGA-1 in AC. An optimum performance occurs at 4 wt% FGA-1 (0.20 g), yielding the highest capacitance.

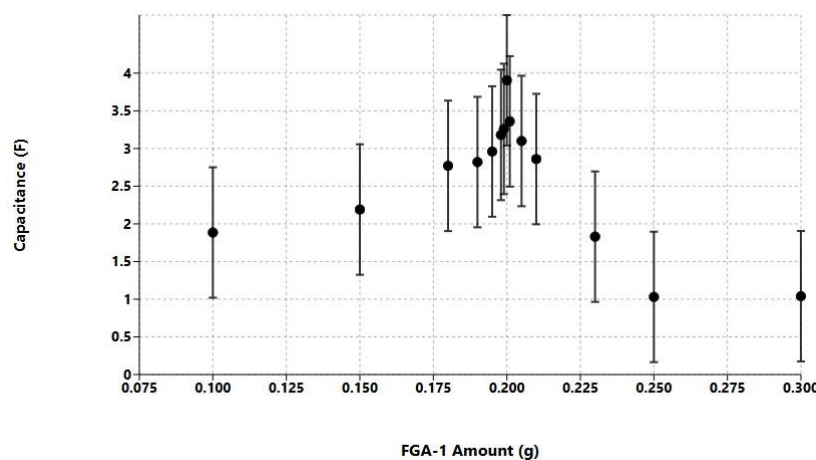


Figure 7. Variation in measured capacitance with increasing FGA-1 content.

Figure 8 compares the cyclic voltammograms of supercapacitor cells made from AC alone versus AC:FGA-1 (at 4% FGA-1). The AC:FGA-1 cell shows significantly higher capacitance (2.935 F, or 172.6 F g⁻¹) compared to the AC-only device (0.735 F, or 45.95 F g⁻¹). Ten devices with the optimal loading of FGA-1 gave an average

capacitance of 4.190 ± 0.866 F, confirming repeatability. The surface resistance of the electrodes in these ten devices are plotted in Figure 9. These surface resistance measurements reveal a decrease from 184 ± 2 m Ω (AC only) to 52 ± 2 m Ω (AC:FGA-1), reflecting improved conductivity and synergy between FGA-1 and AC.

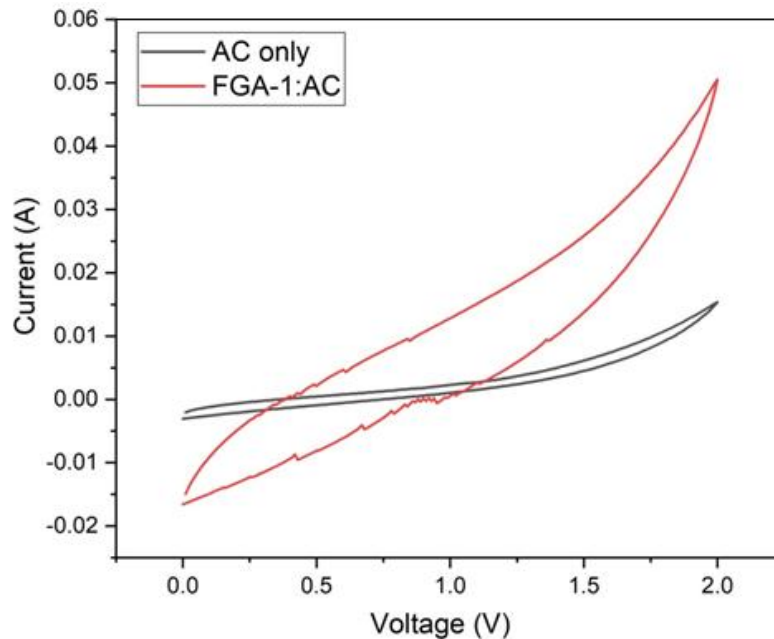


Figure 8. CV curves at 5 mV/s for AC-only and AC:FGA-1 composite supercapacitors.

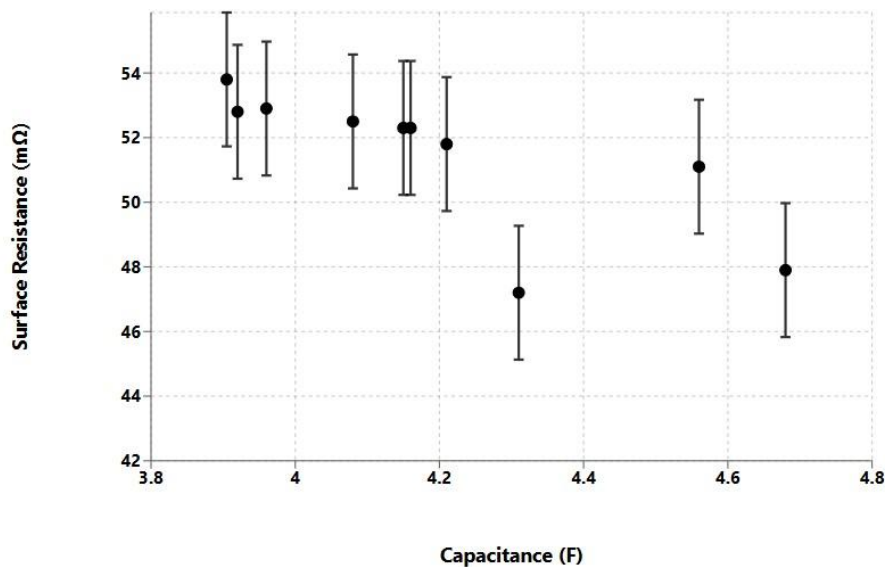


Figure 9. Surface resistance vs. capacitance for AC:FGA-1-based supercapacitors (4 wt% FGA-1).

Although FGA-1 has a modest surface area (~ 165 m 2 g $^{-1}$) relative to AC (~ 1750 – 1980 m 2 g $^{-1}$), the performance improvement likely originates from enhanced electrode wettability and conductivity. This increased wettability ensures better electrolyte penetration and thus more accessible surface area for charge storage in the electric double layer.

Figure 10a compares Nyquist plots of AC-only vs. AC:FGA-1 supercapacitors. The classic semi-circle followed by a 45° -line shape of the Nyquist plot is observed. This plot is related to a capacitor in parallel with a resistor and where the semi-circle touches the real value of impedance (Z') axis yields the d.c. resistance of the device. Figure 10a, thus, shows the composite has a lower impedance than the AC-only electrode. This is in line with the superior conductivity of graphene-based materials [39–42]. Figure 10b shows the Bode phase, where the AC:FGA-1 device has a higher phase angle, indicating a more pronounced capacitive behavior compared to AC-only.

Galvanostatic charge-discharge (GCD) curves at 1.5 A g^{-1} (Figure 10c,d) show that the AC:FGA-1 device reaches higher voltages (2.5 V) than AC-only (0.7 V), consistent with enhanced stability, lower internal resistance, and greater conductivity in the composite [43–49]. From GCD and CV analyses, the composite's specific capacitance is $\sim 189.41 \text{ F g}^{-1}$ (GCD) and $\sim 172.6 \text{ F g}^{-1}$ (CV), while AC-only yields $\sim 52.26 \text{ F g}^{-1}$ (GCD) and $\sim 45.95 \text{ F g}^{-1}$ (CV).

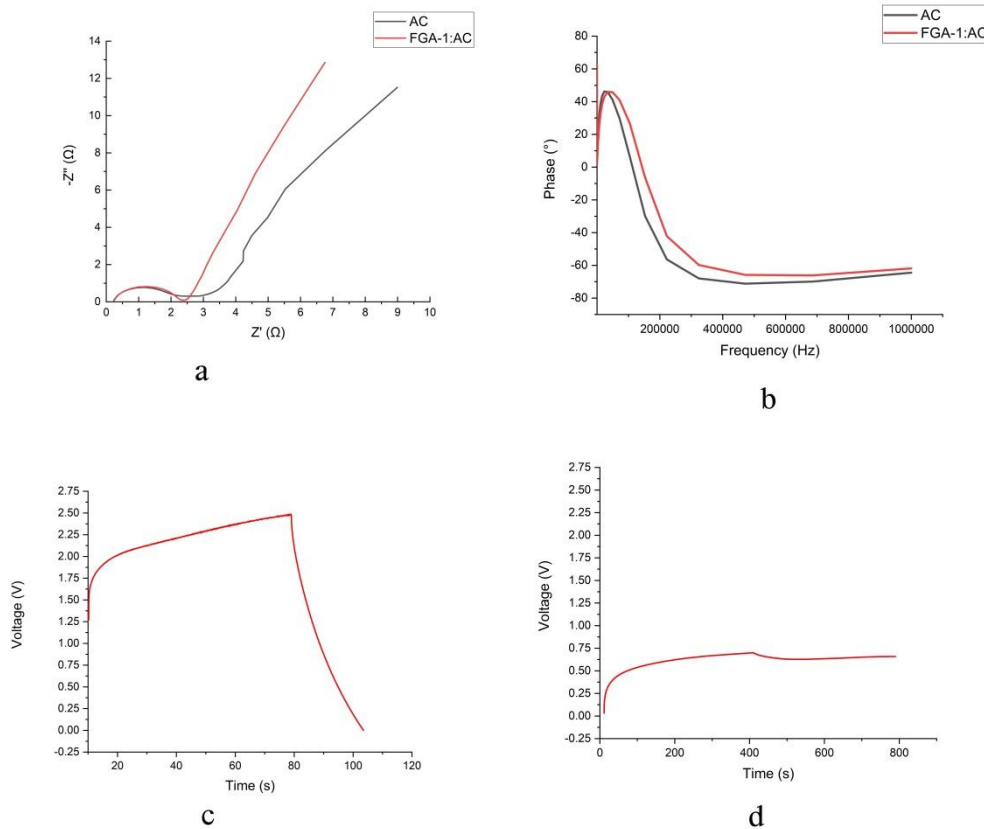


Figure 10. (a) Nyquist plot, (b) Bode phase, (c) GCD curve for AC:FGA-1 at 1.5 A g^{-1} , (d) GCD curve for AC-only at 1.5 A g^{-1} .

4. Conclusions

The experimental results presented here demonstrate that incorporating a small fraction (4 wt%) of Fractal Graphene (FGA-1) into activated carbon electrodes substantially enhances supercapacitor performance. Notably, the composite's lower electrical resistance and faster electrolyte diffusion both contribute to significant increases in specific capacitance—from 45.95 F g^{-1} (AC only) to 172.6 F g^{-1} (AC:FGA-1).

Characterization using UV-Vis, SEM, XRD, and Raman spectroscopy confirms that FGA-1 and AC form a physical mixture without major alterations in crystal structure. The synergy arises primarily from improved wettability and conductivity rather than a simple increase in surface area. Enhanced electrode wettability allows electrolyte penetration into pores, thereby accessing more active sites for charge storage.

Overall, these findings suggest that even a small amount of FGA-1 can enhance the energy density and rate capability of carbon-based supercapacitors, offering a promising pathway for high-performance energy storage devices in applications ranging from consumer electronics to renewable energy systems.

Author Contributions: M.D.: conceptualization, methodology, investigation; software; data curation, writing—original draft preparation; C.K.: data curation, supervision; writing—original draft preparation; A.V.R.S.K.: investigation; data curation, S.G.S.M.N.: investigation; data curation, M.I.U.W.: investigation; data curation; G.R.A.K.: investigation; data curation; R.D.: conceptualization, methodology, writing—reviewing and editing; supervision. All authors have read and agreed to the published version of the manuscript.

Funding: This research received no external funding.

Institutional Review Board Statement: Not applicable.

Informed Consent Statement: Not applicable.

Data Availability Statement: Data is available from M.D. at maithri.d@gmail.com.

Acknowledgments: The authors gratefully acknowledge the National Institute of Fundamental Studies, Hantana, Sri Lanka, for providing the facilities to conduct this research. We extend special thanks to HydroGraph Clean Power Inc. (Toronto, Canada) and CEO Kjirstin Breure for supplying the Fractal Graphene used in this study. We also thank Haycarb PLC for providing the HCE 202 AC sample.

Conflicts of Interest: R.D. declares a conflict of interest in that he holds an executive position in Hydrograph Clean Power Inc.

References

1. Li, J.; Xiao, T.; Yu, X.; Wang, M. Graphene-based composites for supercapacitors. *J. Phys. Conf. Ser. Inst. Phys.* **2022**, *2393*, 012005. <https://doi.org/10.1088/1742-6596/2393/1/012005>.
2. Achkari, O. and Fadar, A. El. Renewable Energy Storage Technologies - A Review, Proceeding of Engineering and Technology -PET, 2018, Vol 35, pp 60-79.
3. Tromly, K. Renewable Energy: An Overview. Energy Efficiency and Renewable Energy Clearinghouse (EREC) Brochure. DOE/GO-102001-1102. FS175, March 2001.
4. Sayed, E.T.; Olabi, A.G.; Alami, A.H.; Radwan, A.; Mdallal, A.; Rezk, A.; Abdelkareem, M.A. Renewable Energy and Energy Storage Systems. *Energies* **2023**, *16*, 1415. <https://doi.org/10.3390/en16031415>.
5. Yunus, A.M.S.; Swasti, S. Purwito, Overview of Hysteresis Current Controller Application in Renewable Energy Based Power Systems. *IOP Conf. Ser. Mater. Sci. Eng.* **2019**, *536*, 012048. <https://doi.org/10.1088/1757-899X/536/1/012048>.
6. Sridhar, S.; Salkuti, S.R. Development and Future Scope of Renewable Energy and Energy Storage Systems. *Smart Cities* **2022**, *5*, 668–699. <https://doi.org/10.3390/smartcities5020035>.
7. Uno, M. Supercapacitor-Based Electrical Energy Storage System. *Energy Storage Emerg. Era Smart Grids* **2011**, *10*, 18667. <https://doi.org/10.5772/18667>.
8. Vukajlović, N.; Milićević, D.; Dumnić, B.; Popadić, B. Comparative analysis of the supercapacitor influence on lithium battery cycle life in electric vehicle energy storage. *J. Energy Storage* **2020**, *31*, 101603. <https://doi.org/10.1016/j.est.2020.101603>.
9. Olabi, A.G.; Abbas, Q.; Abdelkareem, M.A.; Alami, A.H.; Mirzaeian, M.; Sayed, E.T. Carbon-Based Materials for Supercapacitors: Recent Progress, Challenges and Barriers. *Batteries* **2022**, *9*, 19. <https://doi.org/10.3390/batteries9010019>.
10. Sharma, K.; Arora, A.; Tripathi, S.K. Tripathi, Review of supercapacitors: Materials and devices. *J. Energy Storage* **2019**, *21*, 801–825. <https://doi.org/10.1016/j.est.2019.01.010>.
11. Jalal, N.I.; Ibrahim, R.I.; Oudah, M.K. A review on Supercapacitors: Types and components. *J. Phys.* **2021**, *1973*, 012015. <https://doi.org/10.1088/1742-6596/1973/1/012015>.
12. Halper, M.S.; Ellenbogen, J.C. *Supercapacitors: A Brief Overview*; MITRE Nanosystems Group: Tysons, VA, USA, 2006.
13. Senthilkumar, S.T.; Selvan, R.K.; Lee, Y.S.; Melo, J.S. Electric double layer capacitor and its improved specific capacitance using redox additive electrolyte. *J. Mater. Chem. A* **2013**, *1*, 1086–1095. <https://doi.org/10.1039/c2ta00210h>.
14. Borenstein, A.; Hanna, O.; Attias, R.; Luski, S.; Brousse, T.; Aurbach, D. Carbon-based composite materials for supercapacitor electrodes: A review. *J. Mater. Chem. A* **2017**, *5*, 12653–12672. <https://doi.org/10.1039/c7ta00863e>.
15. Fields, R.; Lei, C.; Markoulidis, F.; Lekakou, C. The Composite Supercapacitor. *Energy Technol.* **2016**, *4*, 517–525. <https://doi.org/10.1002/ente.201500328>.
16. Thomas, S.; Abraham, J.; Parambil, A.M.; Krishnan, A.; Maria, H.J.; Ilschner, B.; Lees, J.K.; Dhingra, A.K.; McCullough, R.L. Composite Materials. In *Ullmann's Encyclopedia of Industrial Chemistry*; Wiley: New York, NY, USA, 2016; pp. 1–44. https://doi.org/10.1002/14356007.a07_369.pub2.
17. Wang, G.; Wang, H.; Zhong, B.; Zhang, L.; Zhang, J. *Supercapacitors' Applications*; Taylor & Francis Group, LLC: Oxford, UK, 2016; pp. 479–492. <https://doi.org/10.1201/B19061-27>.
18. Ernst, A.J.; Ansah, I.; Bachus, K.; Kporxah, C.; Tomomewo, O.S. The Role of Energy Storage in the Evolution of Renewable Energy and Its Effect on the Environment. *Am. J. Energy Res.* **2023**, *11*, 128–143. <https://doi.org/10.12691/ajer-11-3-4>.
19. Ke, Q.; Wang, J. Graphene-based materials for supercapacitor electrodes—A review. *J. Mater.* **2016**, *2*, 37–54. <https://doi.org/10.1016/j.jmat.2016.01.001>.
20. Stoller, M.D.; Park, S.; Yanwu, Z.; An, J.; Ruoff, R.S. Graphene-Based ultracapacitors. *Nano Lett.* **2008**, *8*, 3498–3502. <https://doi.org/10.1021/nl802558y>.
21. Moreno-Jimenez, D.A.; Kim, K.Y. Enhanced wettability improves catalytic activity of nickel-functionalized activated carbon cathode for hydrogen production in microbial electrolysis cells. *Bioresour. Technol.* **2022**, *350*, 126881. <https://doi.org/10.1016/J.BIORTECH.2022.126881>.

22. Dissanayake, S.M.B.; Wimalasena, I.G.K.J.; Keppetipola, N.M.; Karunarathne, B.C.; Medagedara, A.D.T.; Cojocar, L.; Uchida, S.; Rajapakse, R.M.G.; Tennakone, K.; Yoshimura, M.; et al. Effect of Triton X-100 surfactant concentration on the wettability of polyethylene-based separators used in supercapacitors. *J. Sci. Adv. Mater. Devices* **2024**, *9*, 100801. <https://doi.org/10.1016/J.JSAM.2024.100801>.
23. Ndagijimana, P.; Rong, H.; Ndokoye, P.; Mwizerwa, J.P.; Nkinahamira, F.; Luo, S.; Guo, D.; Cui, B. A review on activated carbon/graphene composite-based materials: Synthesis and applications. *J. Clean. Prod.* **2023**, *417*, 138006. <https://doi.org/10.1016/J.JCLEPRO.2023.138006>.
24. Dujearic-Stephane, K.; Gupta, M.; Kumar, A.; Sharma, V.; Pandit, S.; Bocchetta, P.; Kumar, Y. The effect of modifications of activated carbon materials on the capacitive performance: Surface, microstructure, and wettability. *J. Compos. Sci.* **2021**, *5*, 66. <https://doi.org/10.3390/jcs5030066>.
25. Ntakirutimana, S.; Tan, W.; Wang, Y. Enhanced surface activity of activated carbon by surfactants synergism. *RSC Adv.* **2019**, *9*, 26519–26531. <https://doi.org/10.1039/C9RA04521J>.
26. Nepal, A.; Singh, G.P.; Flanders, B.N.; Sorensen, C.M. One-step synthesis of graphene via catalyst-free gas-phase hydrocarbon detonation. *Nanotechnology* **2013**, *24*, 245602. <https://doi.org/10.1088/0957-4484/24/24/245602>.
27. Wright, J.P.; Sigdel, S.; Corkill, S.; Covarrubias, J.; LeBan, L.; Nepal, A.; Li, J.; Divigalpitiya, R.; Bossmann, S.H.; Sorensen, C.M. Synthesis of turbostratic nanoscale graphene via chamber detonation of oxygen/acetylene mixtures. *Nano Sel.* **2022**, *3*, 1054–1068. <https://doi.org/10.1002/nano.202100305>.
28. Stiver, W.; Mackay, D. Linear Superposition in Modelling Contaminant Behaviour in Aquatic Systems. *Water Res.* **1995**, *29*, 329–335.
29. Hou, D.; Li, K.; Ma, R.; Liu, Q. Influence of order degree of coaly graphite on its structure change during preparation of graphene oxide. *J. Mater.* **2020**, *6*, 628–641. <https://doi.org/10.1016/j.jmat.2020.04.009>.
30. Sadezky, A.; Muckenhuber, H.; Grothe, H.; Niessner, R.; Pöschl, U. Raman microspectroscopy of soot and related carbonaceous materials: Spectral analysis and structural information. *Carbon* **2005**, *43*, 1731–1742. <https://doi.org/10.1016/j.carbon.2005.02.018>.
31. Judai, K.; Iguchi, N.; Hatakeyama, Y. Low-Temperature Production of Genuinely Amorphous Carbon from Highly Reactive Nanoacetylide Precursors. *J. Chem.* **2016**, *2016*, 7840687. <https://doi.org/10.1155/2016/7840687>.
32. Bakhia, T.; Khamizov, R.K.; Bavizhev, Z.R.; Bavizhev, M.D.; Konov, M.A.; Kozlov, D.A.; Tikhonova, S.A.; Maslakov, K.I.; Ashurov, M.S.; Melezhik, A.V.; et al. Composite graphene-containing porous materials from carbon for capacitive deionization of water. *Molecules* **2020**, *25*, 2620. <https://doi.org/10.3390/molecules25112620>.
33. Folaranmi, G.; Bechelany, M.; Sifat, P.; Cretin, M.; Zaviska, F. Comparative investigation of activated carbon electrode and a novel activated carbon/graphene oxide composite electrode for an enhanced capacitive deionization. *Materials* **2020**, *13*, 5185. <https://doi.org/10.3390/ma13225185>.
34. Chibowski, E.; Hołysz, L. On the use of Washburn's equation for contact angle determination. *J. Adhes. Sci. Technol.* **1997**, *11*, 1289–1301. <https://doi.org/10.1163/156856197X00147>.
35. Liu, T.; Wang, K.; Chen, Y.; Zhao, S.; Han, Y. Dominant role of wettability in improving the specific capacitance. *Green Energy Environ.* **2019**, *4*, 171–179. <https://doi.org/10.1016/j.gee.2019.01.010>.
36. Gromadskyi, D.G.; Chae, J.H.; Norman, S.A.; Chen, G.Z. Correlation of energy storage performance of supercapacitor with iso-propanol improved wettability of aqueous electrolyte on activated carbon electrodes of various apparent densities. *Appl. Energy* **2015**, *159*, 39–50. <https://doi.org/10.1016/j.apenergy.2015.08.108>.
37. Zhao, Y.; Geng, Z.; Sun, W. Activated Carbon-Based Supercapacitors with High Gravimetric and Volumetric Capacitance at Commercial-Level Mass Loading. *Energy Technol.* **2023**, *11*, 2300373. <https://doi.org/10.1002/ente.202300373>.
38. Du, X.; Wang, S.; Liu, Y.; Lu, M.; Wu, K.; Lu, M. Self-assembly of free-standing hybrid film based on graphene and zinc oxide nanoflakes for high-performance supercapacitors. *J. Solid State Chem.* **2019**, *277*, 441–447. <https://doi.org/10.1016/j.jssc.2019.06.003>.
39. Li, Y.; Shang, T.-X.; Gao, J.-M.; Jin, X.-J. Nitrogen-doped activated carbon/graphene composites as high-performance supercapacitor electrodes. *RSC Adv.* **2017**, *7*, 19098–19105. <https://doi.org/10.1039/C7RA00132K>.
40. Gürten Inal, İ. Scalable activated carbon/graphene based supercapacitors with improved capacitance retention at high current densities. *Turk. J. Chem.* **2021**, *45*, 927–941. <https://doi.org/10.3906/kim-2012-39>.
41. Rahim, A.H.A.; Ramli, N.; Nordin, A.N.; Wahab, M.F.A. Supercapacitor Performance with Activated Carbon and Graphene Aerogel Composite Electrodes. *Int. J. Nanoelectron. Mater.* **2022**, *15*, 139–154.
42. Rahim, A.H.A.; Ramli, N.; Nordin, A.N.; Wahab, M.F.A. Supercapacitor performance with activated carbon and graphene nanoplatelets composite electrodes, and insights from the equivalent circuit model. *Carbon Trends* **2021**, *5*, 100101. <https://doi.org/10.1016/j.cartre.2021.100101>.
43. Barzegar, F.; Bello, A.; Fashedemi, O.O.; Dangbegnon, J.K.; Momodu, D.Y.; Taghizadeh, F.; Manyala, N. Synthesis of 3D porous carbon based on cheap polymers and graphene foam for high-performance electrochemical capacitors.

- Electrochim. Acta* **2015**, 180, 442–450. <https://doi.org/10.1016/j.electacta.2015.08.148>.
44. Arunkumar, M.; Paul, A. Importance of Electrode Preparation Methodologies in Supercapacitor Applications. *ACS Omega* **2017**, 2, 8039–8050. <https://doi.org/10.1021/acsomega.7b01275>.
 45. Lazanas, A.C.; Prodromidis, M.I. Electrochemical Impedance Spectroscopy—A Tutorial. *ACS Meas. Sci. Au* **2023**, 3, 162–193. <https://doi.org/10.1021/acsmesuresciau.2c00070>.
 46. ABID, M.A.A.M.; Radzi, M.I.; Mupit, M.; Osman, H.; Munawar, R.F.; Samat, K.F.; Islam, M.R. Cyclic Voltammetry and Galvanostatic Charge-Discharge Analyses of Polyaniline/Graphene Oxide Nanocomposite based Supercapacitor. *Malays. J. Compos. Sci. Manuf.* **2020**, 3, 14–26. <https://doi.org/10.37934/mjcs.3.1.1426>.
 47. Gunday, S.T.; Cevik, E.; Anil, I.; Alagha, O.; Sabit, H.; Bozkurt, A. Symmetric Supercapacitor Application of Anhydrous Gel Electrolytes Comprising Doped Tetrazole Terminated Flexible Spacers. *Macromol. Res.* **2020**, 28, 1074–1081. <https://doi.org/10.1007/s13233-020-8150-9>.
 48. Chen, L.; Bai, H.; Huang, Z.; Li, L. Mechanism investigation and suppression of self-discharge in active electrolyte enhanced supercapacitors. *Energy Environ. Sci.* **2014**, 7, 1750–1759. <https://doi.org/10.1039/C4EE00002A>.
 49. Azman, N.H.N.; Nazir, M.S.M.M.; Ngee, L.H.; Sulaiman, Y. Graphene-based ternary composites for supercapacitors. *Int. J. Energy Res.* **2018**, 42, 2104–2116. <https://doi.org/10.1002/er.4001>.